Nanoscale

Check for updates

Rapid reaction of MoS$_2$ nanosheets with Pb^{2+} and Pb^{4+} ions in solution†

Biswajit Mondal,‡ Ananthu Mahendranath,‡ Anirban Som, [ID] Sandeep Bose, Tripti Ahuja, Avula Anil Kumar, Jyotirmoy Ghosh and Thalappil Pradeep [ID] *

Understanding the chemical changes happening to nanostructures during a process is vital in selecting them for applications. Here, we investigated the difference in the reactivity of the bulk and nanoscale forms of molybdenum disulfide (MoS$_2$) in solution with lead ions (Pb^{2+} and Pb^{4+}) as probes, at room temperature. While the bulk form did not show any reactivity in the experimental timescale, the two-dimensional (2D) nanoscale form showed not only reactivity but also quite rapid kinetics that resulted in the formation of distinct products, principally PbMoO$_4$ with anion substitution, in a few seconds. Depending on the charge state of the cation, and the pH of the reaction mixture, two different kinds of morphologies of the same reaction product were formed. Furthermore, we demonstrate that this unusual reactivity of the MoS$_2$ nanosheets (NSs) was retained in its supported form and hence, such supported materials can be effective for the abstraction of toxic lead from water, with fast kinetics.

Introduction

Inorganic analogues of graphene, due to their unusual electrical,[1–4] electronic,[5–8] magnetic,[9–11] and catalytic properties,[12–19] are fascinating materials which have made great inroads into materials science in the recent past. While their novel physical properties have been fascinating, most investigations have left the nanostructures undisturbed. As modified physical properties have been inherent to nanosystems, retention of the structure has been essential for the properties. Likely chemical changes in them during the processes have been of limited concern. MoS$_2$ has been used as a hydrodesulphurization catalyst[20–22] which requires the edge sites to be catalytically active. The process by itself leaves the overall structure chemically unchanged although transient changes occur during the hydrodesulphurization event. From various investigations, it is now clear that the chemical properties of nanoscale materials can be distinctly different from the bulk and such a reactivity could make the inorganic analogues of graphene new reagents.[23,24]

Water is becoming increasingly contaminated by a wide variety of pollutants, mainly from agricultural and industrial sources. Among them, heavy metal contamination in water is a worldwide concern, because of their extreme toxicity. Many techniques have been employed for their removal such as ion exchange, electrochemical precipitation, membrane separation, adsorption, chemical precipitation, *etc*. Among them, adsorption is the most promising one because of its ease of operation, simplicity in the design of the filter and low cost. In this context, the use of new materials[25–28] is becoming increasingly important and the interaction of these materials with heavy metals is an interesting topic to look into.

With these objectives, we explored the difference in the chemical reactivity of bulk MoS$_2$ (b-MoS$_2$) *versus* its chemically exfoliated nanoscale analogue (n-MoS$_2$) with Pb^{2+} and Pb^{4+} in solution, at room temperature. While b-MoS$_2$ turned out to be completely unreactive, n-MoS$_2$ rapidly transformed to PbMoO$_{4-x}$S$_x$ in a reaction utilizing hydroxyl ions in the solution. The micron-scale particles of PbMoO$_{4-x}$S$_x$ could be annealed in solution resulting in interesting morphologies. We utilized reactions of n-MoS$_2$ anchored on oxide supports as an effective means to scavenge Pb^{2+} and Pb^{4+} in solution, creating novel media for heavy metal remediation in waste water.

Experimental

Materials

All the chemicals are commercially available and were used without further purification. Molybdenum disulfide powder (MoS$_2$) and 1.6 M *n*-butyllithium in hexane were purchased from Sigma Aldrich. Lead acetate trihydrate (Pb(OAc)$_2$·3H$_2$O) and lead dioxide (PbO$_2$) were purchased from RANKEM.

Synthesis of chemically exfoliated MoS₂ nanosheets

The synthesis of chemically exfoliated MoS_2 nanosheets (n-MoS_2) was carried out using a conventional chemical exfoliation method.[29] Under an inert atmosphere of argon, 3 mL of 1.6 M n-butyllithium in hexane was added to 300 mg of bulk MoS_2 (powder) taken in a round-bottom flask. The system was left with constant stirring for nearly 48 h, maintaining the inert atmosphere. After 48 h, the lithium intercalated product (Li_xMoS_2) was collected and washed repeatedly with hexane to remove the unreacted n-butyllithium. 100 mL of distilled water was then added to this intercalated material and the system was sonicated for 1 h using a bath sonicator. Finally, this aqueous dispersion of n-MoS_2 was centrifuged at 18 000 rpm for 15 minutes to remove the unexfoliated MoS_2 as a precipitate. The supernatant containing the n-MoS_2 NSs was used for further studies.

MoS_2 NSs of varying thickness were prepared as follows. The exfoliated MoS_2 dispersion was centrifuged at various speeds to obtain MoS_2 NSs of varying thickness. First, the dispersion was centrifuged at 5000 rpm for 10 minutes to remove the un-exfoliated MoS_2 (b-MoS_2). When the supernatant was centrifuged at 10 000 rpm, the precipitate contained 5–8 layers of MoS_2 NSs. The supernatant upon further centrifugation at 15 000 rpm gave a precipitate containing NSs of 3–5 layers (data are given in the ESI†).

Reaction of n-MoS₂ with Pb²⁺

4 ml of as-prepared n-MoS_2 (2–3 layers) dispersion in water (4.6 mM, in terms of Mo concentration) was taken in a reaction bottle, to which 1 mL (22 mM) of lead acetate solution was added. A white precipitate was observed immediately, upon the addition of $Pb(OAc)_2$. The total volume of the reaction mixture was 5 mL and the final concentrations of MoS_2 and $Pb(OAc)_2$ in the solution were 3.7 mM and 4.4 mM, respectively. The reaction was continued for 6 h under constant magnetic stirring and was monitored by UV/Vis spectroscopy (Fig. S1†). The reaction mixture was then centrifuged at 3000 rpm for 5 min. The precipitate was collected and washed repeatedly with H_2O to remove the excess reactants. Concentration-dependent reactions were performed by keeping the n-MoS_2 concentration the same (4 mL, 4.2 mM) and varying the $Pb(OAc)_2$ concentration (22 mM, 44 mM, 66 mM and 88 mM). The reactions were monitored using UV/Vis spectroscopy (Fig. S2†).

The reactivity of MoS_2 NSs depends on the number of layers of MoS_2 NSs. It is observed that MoS_2 NSs with ≤5 layers are unreactive towards lead ions (Fig. S3†).

Reaction of n-MoS₂ with Pb⁴⁺

A reaction with Pb^{4+} was carried out in a similar fashion to the case of Pb^{2+}, except for the use of a mixed solvent (H_2O : acetic acid 1 : 1) as the Pb^{4+} source used (PbO_2) is not soluble in H_2O.

The reactions were also carried out in tap water to observe the feasibility of these reactions in such an environment.

Results and discussion

The chemical exfoliation of MoS_2 NSs involved two steps. The first step involved the intercalation and in the second step, the intercalated product was exfoliated in water. The quality of the NSs was examined by spectroscopic and microscopic techniques. Typically, n-MoS_2 was 200 to 1000 nm in length and had an average thickness of 2–3 layers (Fig. 1A). The UV-visible absorption spectra (inset of Fig. 1A) of the n-MoS_2 dispersion show the characteristic peaks at 435 nm, 611 nm, and 668 nm.[30,31] The two features between 600–700 nm are known to arise from the direct transitions occurring at the K point of the Brillouin zone.[32] The HRTEM image (Fig. 1B) of the n-MoS_2 showed a well resolved hexagonal lattice structure and a lattice spacing of 0.27 nm corresponding to the $d(100)$ plane.[33] The Fast Fourier Transform (FFT) pattern of the HRTEM image (inset, Fig. 1B) showed the expected hexagonal pattern for graphenic equivalents.

The quality of the NSs was further probed using Raman spectroscopy. On comparing the Raman spectra (Fig. 1C) of b-MoS_2 with n-MoS_2, we find that the peak difference of A_{1g} and E_{2g} modes had decreased (~19 cm^{-1}) in the latter. This difference corresponds to a thickness of approximately 2–3 layers in n-MoS_2. Also the FWHM for the A_{1g} mode has increased in n-MoS_2 (Fig. 1C) suggesting the successful exfoliation of b-MoS_2.[34,35]

The reaction products between Pb^{2+}/Pb^{4+} and MoS_2, in its bulk and 2D nanoscale forms were investigated. Solutions of Pb^{2+} and Pb^{4+}, added to the b-MoS_2 (powder) separately, remained unreactive for an extended period of time (24 h) without any visible change in either the colour of the dispersion or the morphology and chemical composition of the MoS_2 particles. The inactiveness of b-MoS_2 towards lead ions can be explained by thermochemical values (ΔG_f° values of MoS_2 and $PbMoO_4$ are −248.7 kJ mol^{-1} (ref. 36) and −89.12 kJ mol^{-1} (ref. 37), respectively). In stark contrast to this behaviour of b-MoS_2, n-MoS_2 showed an immediate reaction with both the ions.

Upon mixing lead ions (both Pb^{2+} and Pb^{4+}, separately) with n-MoS_2 dispersion, an immediate visual change was noticed. The light green colour of the n-MoS_2 dispersion turned milky white, followed by an immediate precipitation of the reaction products. The white precipitate was collected and washed several times with water to remove any unreacted reactants. Both the ions (Pb^{2+} and Pb^{4+}) gave chemically identical reaction products, however, with different morphologies (Fig. 1D). The white precipitate obtained through the reaction of Pb^{2+} with n-MoS_2 was subjected to powder X-ray diffraction (PXRD) analysis (blue trace, Fig. 2A). The PXRD pattern of the product was similar to the standard PXRD pattern of $PbMoO_4$, along with a set of other peaks. These extra peaks are marked with an asterisk (*). We presumed that these peaks originated from the presence of other phases, probably metastable ones, as these could not be matched with any known phases containing the elements Pb, Mo, O, and S, as confirmed from EDS spectroscopy. To test our hypothesis, the material was then
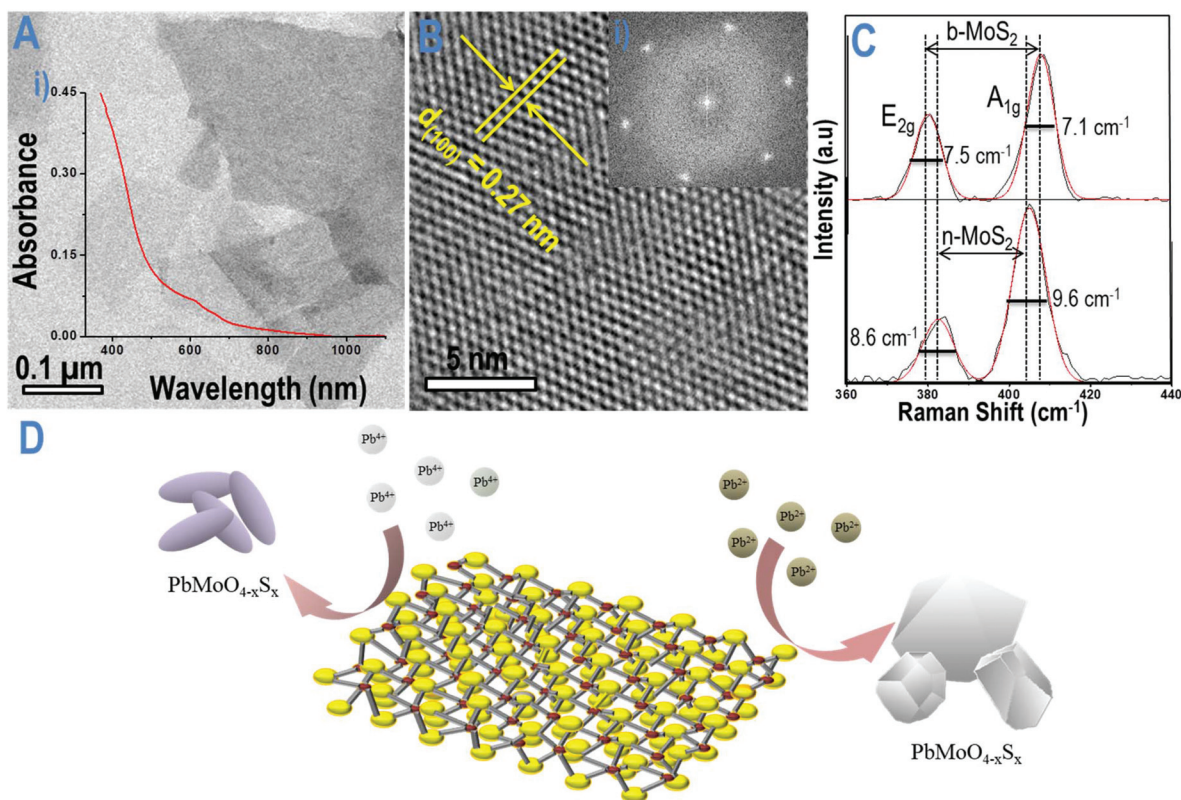
Fig. 1 (A) Representative TEM image of n-MoS$_2$. The optical absorption spectrum is shown in the inset. (B) HRTEM image of NSs. The corresponding FFT pattern is shown in the inset. The lattice plane is marked. (C) Raman spectrum of b-MoS$_2$ (above) and n-MoS$_2$ (below). Peaks have been fitted with Gaussian functions, which indicate an increase in width in the nanoscale form. (D) Schematic of the overall reaction between n-MoS$_2$ and Pb ions (not to scale). Two different morphologies formed by the reaction are shown.

treated hydrothermally at various temperatures with the expectation that these metastable phases will transform into a single, thermodynamically stable phase (Fig. S4†). An exact match with PbMoO$_4$ in the PXRD pattern was observed after 24 h of hydrothermal treatment of the product at 190 °C (black trace, Fig. 2A), proving our hypothesis to be correct. The morphological characterization of this hydrothermally treated product was carried out using an SEM, which confirmed that the size of the microcrystals is of the order of a few microns with an 18-faceted polyhedral morphology (Fig. 2B).[38] The product was further characterized using Raman spectroscopy in the range from 100 to 1000 cm^{-1} (Fig. 2D). The Raman spectrum of the product was dominated by one stretching mode A$_g^3$ at 868.8 cm^{-1}.[39] The two peaks at 767.3 cm^{-1} and 745.7 cm^{-1} can be assigned to the anti-symmetric stretching B$_g^5$ and E$_g^5$ vibrational modes, respectively.[39] The Raman peaks at 351.3 cm^{-1} and 319.1 cm^{-1} corresponded to the weaker B$_g^4$ mode and stronger A$_g^2$/B$_g^3$ modes, respectively.[39] The peaks at 197.1 cm^{-1} and 170.2 cm^{-1} were assigned to E$_g^3$ and A$_g^1$ modes, respectively.[39] The TEM image of the product was obtained at different magnifications, for further characterization (Fig. 2C, E and F). The HRTEM image (Fig. 2E and F) of the product showed the lattice spacing of 0.33 nm corresponding to the d(112) plane which further confirmed the for-

mation of the product. EDS intensity mapping was performed to confirm the presence of all the expected elements (Fig. S5†). A very low intensity of S in the EDS intensity map with a high intensity of Pb, Mo, and O presumably corresponds to the replacement of O positions with S in the PbMoO$_4$ lattice. However, this low degree of S doping does not seem to affect the crystal structure as well as the interplanar distances.

In contrast, a reaction with Pb^{4+} creates PbMoO$_{4-x}$S$_x$ directly, although the particles are much smaller showing a broad PXRD peak. The morphology of the product was completely different in the Pb^{4+} case. To confirm whether this product is indeed the same product as in the Pb^{2+} case with a different morphology, the final reaction product was subjected to PXRD after washing with a mixed solvent (H$_2$O : acetic acid). The obtained PXRD pattern was an exact match with PbMoO$_4$. The product was subjected to hydrothermal treatment under conditions similar to the previous case to ensure that metastable phases are removed. Subsequently, a PXRD measurement was performed. All the peaks of the product became sharper without the disappearance of any, suggesting an increased crystallinity of the product after hydrothermal treatment. SEM images at different magnifications showed a rice grain kind of morphology of the final product (Fig. 3B and C). The blue shift in A$_g^3$ and B$_g^5$ vibrational modes compared to
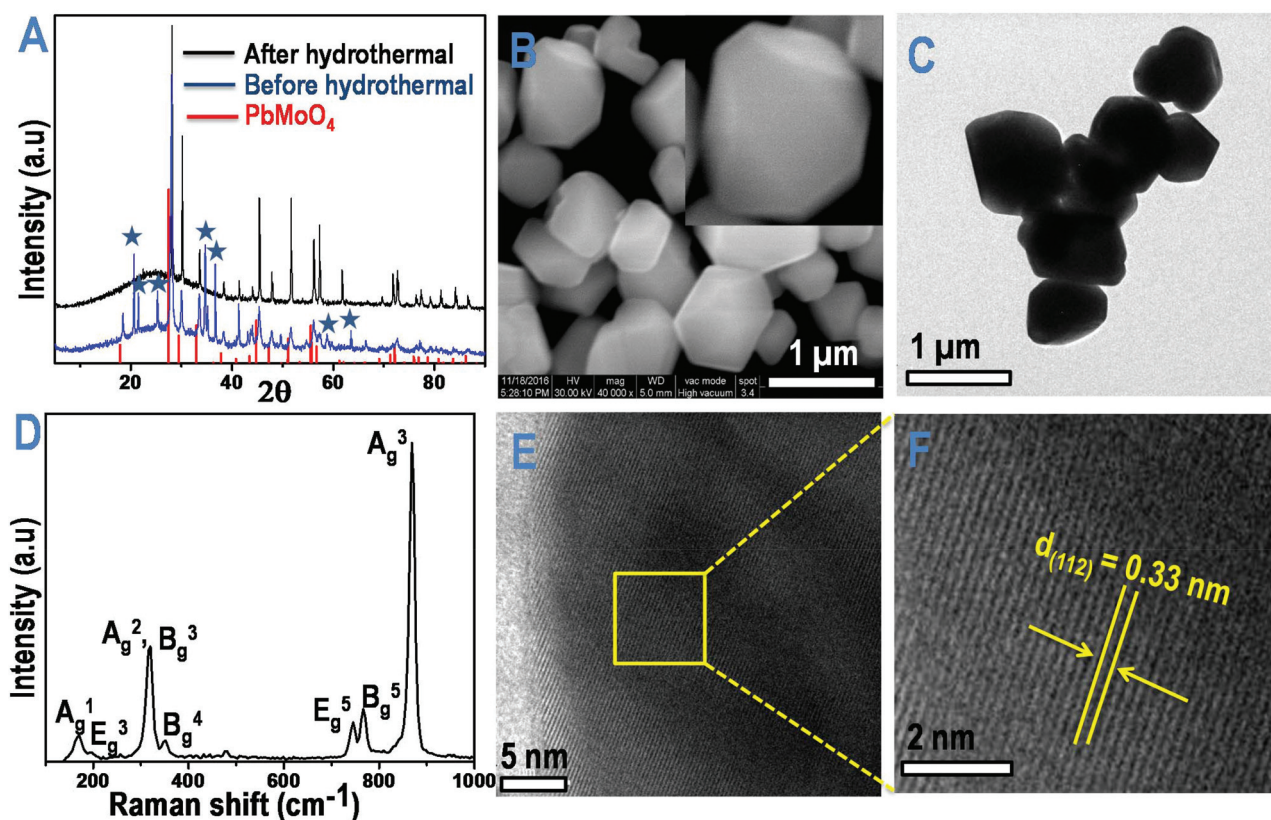
Fig. 2 Characterization of the reaction product of MoS_2 and Pb^{2+} ions. (A) Standard peaks of $PbMoO_4$ (red) are plotted along with the observed XRD pattern before (blue) and after (black) the hydrothermal treatment of the reaction product. (B) SEM image showing a polyhedron morphology of $PbMoO_{4-x}S_x$. The inset shows the SEM image of one such 18-faceted polyhedron. (D) Raman spectrum; TEM and HRTEM images of the same are shown in (C) and (E), respectively. A particular area of image (E) is marked which is magnified in (F).

the same in the MoS_2 + Pb^{2+} case suggests the reduced particle size and nanocrystalline nature of the material (Fig. 3D). These may be inferred from the HRTEM image in Fig. 3F. These also show a lattice spacing of 0.33 nm corresponding to the $d(112)$ plane of $PbMoO_4$.

In order to investigate the stability of the final product with a rice-grain kind of morphology, mechanical grinding of the product was performed using a mortar and pestle. To our surprise, a visible colour change was observed from white to black during grinding (inset of Fig. 4A). A broad feature was seen in the PXRD of the product (Fig. 4A). We attribute this to the formation of smaller particles. The formation of NPs within the range of around 5–50 nm was further confirmed by the TEM image (Fig. 4C). The HRTEM images showed a lattice spacing of 0.33 nm which confirmed that no chemical change occurred during the grinding (Fig. 4D and E). Furthermore, it was confirmed by the Raman spectrum too which showed all the characteristic peaks of $PbMoO_4$ (Fig. 4B).

In order to further confirm the formation of the final product, the chemical states of the elements were analysed using XPS (Fig. 5A–D). The XPS survey spectrum showed that the final product consisted of all the expected elements (Pb, Mo, O, and S) and no impurity peaks were detected (Fig. S6†). The specific scan in the Mo 3d region showed four peaks

corresponding to the presence of two types of oxidation states. The peaks at 229.3 eV and 232.4 eV corresponded to the $3d_{5/2}$ and $3d_{3/2}$ Mo(IV) state, respectively. But the disappearance of one oxidation state in the Mo 3d region was observed after hydrothermal treatment corresponding to the formation of a single phase in the final product. The peaks at 232.1 eV and 235.2 eV were assigned to $3d_{5/2}$ and $3d_{3/2}$ of Mo(VI) in the final product (Fig. 5A).[40] The peaks at 138.7 eV and 143.5 eV were attributed to $4f_{7/2}$ and $4f_{5/2}$ of Pb(II) in $PbMoO_{4-x}S_x$ (Fig. 5B).[40] Another doublet centered at lower binding energy (135.8 eV and 140.2 eV) was assigned to $4f_{7/2}$ and $4f_{5/2}$ of Pb(II), arising due to the presence of another binding site. Fig. 5D shows the XPS at the O_{1s} region with a peak centered at 529.9 eV.[40] Like the final product, the material before the hydrothermal treatment also showed one peak in the O_{1s} region. The presence of dopant S was further confirmed by scanning the S 2p region (Fig. 5C). The two peaks at 161.6 eV and 162.9 eV were assigned to $2p_{3/2}$ and $2p_{1/2}$ of S^{2-} in $PbMoO_{4-x}S_x$.

The chemical reaction involves the conversion of Mo(IV) to Mo(VI) as revealed by XPS. As the starting material is MoS_2, it requires the involvement of oxygen for the formation of the molybdate anion (MoO_4^{2-}). In order to test the origin of oxygen, the reaction was performed at various pH values. It is observed that the reaction occurred only in basic medium
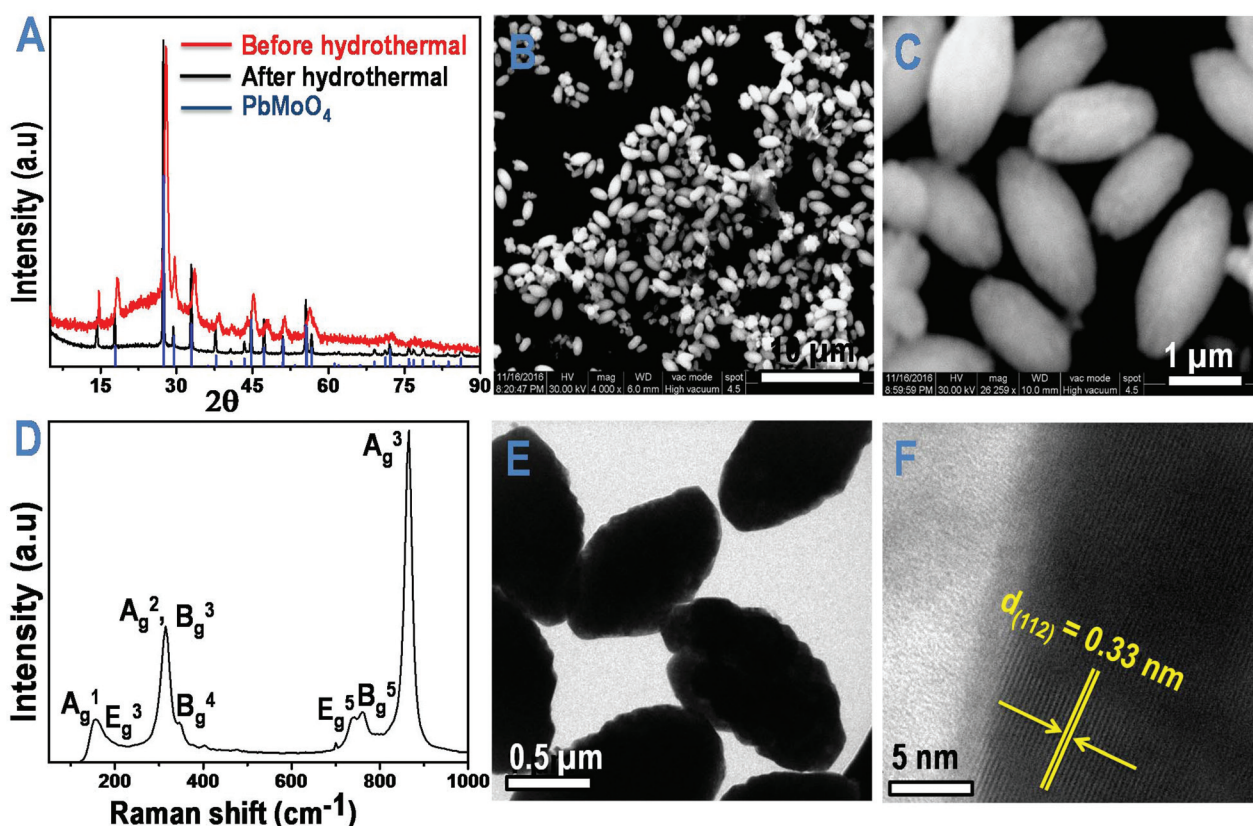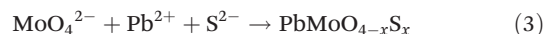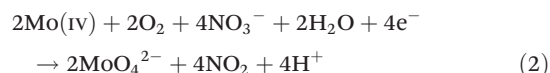
Fig. 3 Characterization of the final reaction product of (MoS_2 + Pb^{4+} reaction). (A) PXRD pattern of the reaction product before (red) and after the hydrothermal treatment (black). SEM images at different magnifications are shown in (B, C). (D) Raman spectrum of the final reaction product. (E, F) TEM and HRTEM images of the same, respectively.

(Fig. S7†). The hydroxyl ions present in the reaction medium are driving the reaction and the decrease in pH during the reaction has confirmed the origin of oxygen in the product. In view of this, we propose a chemical reaction in which Mo(IV) gets oxidized to Mo(VI) driven by OH^- ions while the latter formed H_2O and O_2.

$$4(OH)^- \rightarrow 2H_2O + O_2 + 4e^- \tag{1}$$
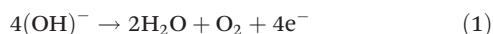
Although this reaction is thermochemically nonspontaneous ($E^0 = -0.4$ V),[41] it can be driven forward due to the involvement of metal ions. We conjecture that acetate ions (coming from lead acetate) are getting reduced to ethanol during the course of the reaction to balance the charge. To prove this, the same reaction was carried out using lead nitrate as a precursor and the formation of NO_2 was examined by *in situ* mass spectrometric detection. Both the reactant solutions were purged with Ar to remove the dissolved O_2, separately. Then the lead nitrate solution was injected into the MoS_2 dispersion taken into an enclosed vessel. The mixtures of gases inside the vessel were analysed after 2 h of reaction using a residual gas analyzer. An increase in ion current was observed for both NO_2 and N_2 due to the increase in the partial pressures of the corresponding gases. When the control (MoS_2 dispersion without lead nitrate solution) was analysed, a reduced ion current for

NO_2 was observed while the ion current for N_2 (background gas) remained the same (Fig. S8†). The control and sample were analysed under the identical reaction conditions to account for some unavoidable leakage. So, the overall reaction for the second and third steps can be written as follows:

$$2Mo(IV) + 2O_2 + 4NO_3^- + 2H_2O + 4e^-$$
$$\rightarrow 2MoO_4^{2-} + 4NO_2 + 4H^+ \tag{2}$$

$$MoO_4^{2-} + Pb^{2+} + S^{2-} \rightarrow PbMoO_{4-x}S_x \tag{3}$$

The experiment suggests the formation of an acid which was again supported by the decrease in the pH during the course of the reaction (Fig. S7†). With tap water, it was observed that as long as lead ions are present, these reactions do occur upon introducing n-MoS_2.

This unusual reactivity can be used for the capture and removal of lead ions from water. In a typical batch experiment, 50 mg of n-MoS_2 adsorbed (0.5 mL, 4.2 mM, in terms of Mo concentration) on alumina or silica was taken in a 200 mL conical flask containing 50 mL of Pb^{2+} solution. The removal % and uptake were calculated using the equations mentioned below:

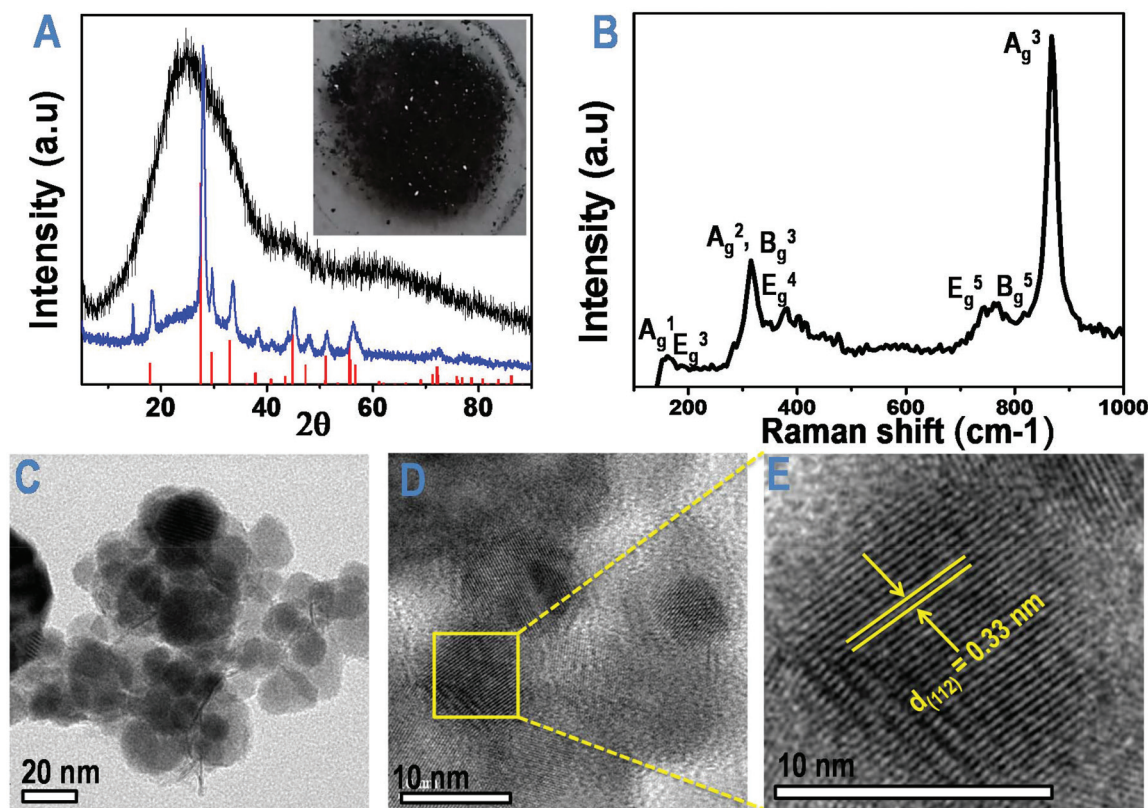$$\text{Removal } \% = \frac{C_0 - C_e}{C_e} \times 100$$

Fig. 4 Conversion of microparticles to nanoparticles by mechanical grinding of the final reaction product. The standard peaks of PbMoO₄ plotted with the XRD pattern of the reaction product before (blue) and after the mechanical grinding (black). The inset shows a photograph of the product after grinding. (B) Raman spectrum of the same showing all the characteristic vibrations. (C, D) TEM and HRTEM images of such particles, respectively. (E) Magnified HRTEM image of one of such particles; the lattice distance is marked.
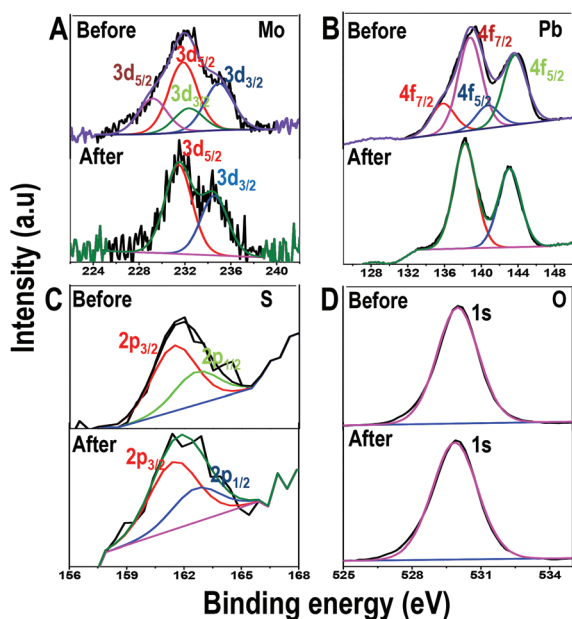

Fig. 5 XPS data to support the formation of $PbMoO_{4-x}S_x$. (A) (i, ii), (B) (i, ii), (C) (i, ii) and (D) (i, ii) correspond to the XPS in the Mo 3d, Pb 4f, S 2p and O₁ₛ regions, before and after the hydrothermal treatment, respectively.

$$Uptake\ (q_e) = \frac{(C_0 - C_e)V}{m}$$

where C_0 and C_e are the initial and equilibrium concentrations of the metal ions, respectively, V is the volume of the solution (L) and m is the mass of the adsorbent (g). The removal capacities of Al₂O₃@n-MoS₂ (282 mg g⁻¹) and SiO₂@MoS₂ (199 mg g⁻¹) nanocomposites were evaluated for Pb²⁺ adsorption using the Freundlich adsorption isotherm. A plot of $\log q_e$ (q_e = heavy metal uptake) vs. $\log C_e$ (C_e = equilibrium concentration of heavy metal ions) showed a straight line with intercepts 0.97, 0.68, 2.45 and 2.3 and slopes 0.47, 0.63, 1.05 and 0.80 for Al₂O₃, SiO₂, n-MoS₂@Al₂O₃ and n-MoS₂@SiO₂, respectively (Fig. 6). The removal capacities of a few other materials, available in the literature, are listed separately (ESI, Table 1†). Batch experiments were performed with different initial concentrations ranging from 1 ppm to 200 ppm. The data were then fitted using the linear form of the Freundlich adsorption isotherm,

$$\log q_e = \log k_f + \frac{1}{n}\log C_e,$$

where k_f is the amount of heavy metal ions adsorbed per g of adsorbent (mg g⁻¹). Although the Freundlich isotherm is not perfectly valid due to the chemical reaction between MoS₂ and
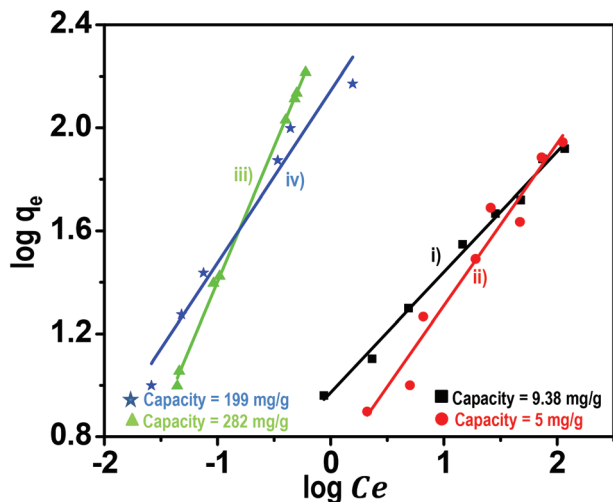
Fig. 6 Equilibrium Pb²⁺ batch adsorption data, fitted using the Freundlich isotherm. (i, ii) Adsorption isotherms using only alumina and silica, respectively. Pb²⁺ removable capacities of Al_2O_3@n-MoS₂ and SiO_2@MoS₂ are shown in (iii, iv), respectively.

Pb²⁺ ions, such models were used in similar cases where MoO_3 reacted with Pb²⁺.[42] Note that supported n-MoS₂ was used, as in such applications, nanoscale materials cannot be employed directly due to potential contamination in the product water. Nanoscale materials for environmental remediation are generally used in the supported form.[43–45]

Conclusions

In conclusion, we present a rapid reaction of n-MoS₂ which does not occur in the bulk form. The reaction of Pb²⁺ and Pb⁴⁺ with n-MoS₂ results in the formation of the same product with different morphologies. Products from each case (Pb²⁺ and Pb⁴⁺) were characterized by spectroscopic and microscopic techniques. The necessity of hydroxyl ions as a source of oxygen is manifested in the course of the reaction. The use of this reaction for removing lead from water has also been demonstrated. These results highlight the relevance of such reactions that occur at room temperature in solution, which may be extended to several other heavy metal ions for environmental remediation. At the same time, the reaction and associated morphologies highlight the need to study a range of chemical processes involving n-MoS₂ and n-MX₂ in general.

Conflicts of interest

There are no conflicts of interest to declare.

Acknowledgements

References

1 I. S. Kim, V. K. Sangwan, D. Jariwala, J. D. Wood, S. Park, K.-S. Chen, F. Shi, F. Ruiz-Zepeda, A. Ponce, M. Jose-Yacaman, V. P. Dravid, T. J. Marks, M. C. Hersam and L. J. Lauhon, *ACS Nano*, 2014, **8**, 10551–10558.

2 J. S. Kim, J. Kim, J. Zhao, S. Kim, J. H. Lee, Y. Jin, H. Choi, B. H. Moon, J. J. Bae, Y. H. Lee and S. C. Lim, *ACS Nano*, 2016, **10**, 7500–7506.

3 T.-Y. Kim, M. Amani, G. H. Ahn, Y. Song, A. Javey, S. Chung and T. Lee, *ACS Nano*, 2016, **10**, 2819–2826.

4 S. Najmaei, M. Amani, M. L. Chin, Z. Liu, A. G. Birdwell, T. P. O'Regan, P. M. Ajayan, M. Dubey and J. Lou, *ACS Nano*, 2014, **8**, 7930–7937.

5 Z. Yin, H. Li, H. Li, L. Jiang, Y. Shi, Y. Sun, G. Lu, Q. Zhang, X. Chen and H. Zhang, *ACS Nano*, 2012, **6**, 74–80.

6 X.-L. Wei, H. Zhang, G.-C. Guo, X.-B. Li, W.-M. Lau and L.-M. Liu, *J. Mater. Chem. A*, 2014, **2**, 2101–2109.

7 A. Steinhoff, M. Roesner, F. Jahnke, T. O. Wehling and C. Gies, *Nano Lett.*, 2014, **14**, 3743–3748.

8 B. Radisavljevic, A. Radenovic, J. Brivio, V. Giacometti and A. Kis, *Nat. Nanotechnol.*, 2011, **6**, 147–150.

9 S. Tongay, S. S. Varnoosfaderani, B. R. Appleton, J. Wu and A. F. Hebard, *Appl. Phys. Lett.*, 2012, **101**, 123105.

10 N. Gao, Y. Guo, S. Zhou, Y. Bai and J. Zhao, *J. Phys. Chem. C*, 2017, **121**, 12261–12269.

11 M. Saab and P. Raybaud, *J. Phys. Chem. C*, 2016, **120**, 10691–10697.

12 Y. Pi, Z. Li, D. Xu, J. Liu, Y. Li, F. Zhang, G. Zhang, W. Peng and X. Fan, *ACS Sustainable Chem. Eng.*, 2017, **5**, 5175–5182.

13 D. Gopalakrishnan, D. Damien, B. Li, H. Gullappalli, V. K. Pillai, P. M. Ajayan and M. M. Shaijumon, *Chem. Commun.*, 2015, **51**, 6293–6296.

14 L. Ma, Y. Hu, G. Zhu, R. Chen, T. Chen, H. Lu, Y. Wang, J. Liang, H. Liu, C. Yan, Z. Tie, Z. Jin and J. Liu, *Chem. Mater.*, 2016, **28**, 5733–5742.

15 Y. Li, H. Wang, L. Xie, Y. Liang, G. Hong and H. Dai, *Condens. Matter*, 2011, 1–9.

16 M. A. Lukowski, A. S. Daniel, F. Meng, A. Forticaux, L. Li and S. Jin, *J. Am. Chem. Soc.*, 2013, **135**, 10274–10277.

17 D. Voiry, M. Salehi, R. Silva, T. Fujita, M. Chen, T. Asefa, V. B. Shenoy, G. Eda and M. Chhowalla, *Nano Lett.*, 2013, **13**, 6222–6227.

18 J. Liang, J. Li, H. Zhu, Y. Han, Y. Wang, C. Wang, Z. Jin, G. Zhang and J. Liu, *Nanoscale*, 2016, **8**, 16017–16025.

19 H. Li, C. Tsai, A. L. Koh, L. Cai, A. W. Contryman, A. H. Fragapane, J. Zhao, H. S. Han, H. C. Manoharan, F. Abild-Pedersen, J. K. Norskov and X. Zheng, *Nat. Mater.*, 2016, **15**, 48–53.

20 V. H. J. de Beer, J. G. J. Dahlmans and J. G. M. Smeets, *J. Catal.*, 1976, **42**, 467–470.

21 J.-F. Paul and E. Payen, *J. Phys. Chem. B*, 2003, **107**, 4057–4064.

22 C. T. Tye and K. J. Smith, *Top. Catal.*, 2006, **37**, 129–135.

23 Z. Chen, A. J. Forman and T. F. Jaramillo, *J. Phys. Chem. C*, 2013, **117**, 9713–9722.

24 B. Mondal, A. Som, I. Chakraborty, A. Baksi, D. Sarkar and T. Pradeep, *Nanoscale*, 2016, **8**, 10282–10290.

25 X. Gu, Y. Yang, Y. Hu, M. Hu and C. Wang, *ACS Sustainable Chem. Eng.*, 2015, **3**, 1056–1065.

26 P. Liu, T. Yan, L. Shi, H. S. Park, X. Chen, Z. Zhao and D. Zhang, *J. Mater. Chem. A*, 2017, **5**, 13907–13943.

27 L. Liu, X. Guo, R. Tallon, X. Huang and J. Chen, *Chem. Commun.*, 2017, **53**, 881–884.

28 P. Liu, T. Yan, J. Zhang, L. Shi and D. Zhang, *J. Mater. Chem. A*, 2017, **5**, 14748–14757.

29 L. Yuwen, F. Xu, B. Xue, Z. Luo, Q. Zhang, B. Bao, S. Su, L. Weng, W. Huang and L. Wang, *Nanoscale*, 2014, **6**, 5762–5769.

30 H.-L. Liu, C.-C. Shen, S.-H. Su, C.-L. Hsu, M.-Y. Li and L.-J. Li, *Appl. Phys. Lett.*, 2014, **105**, 201905.

31 K. Wang, J. Wang, J. Fan, M. Lotya, A. O'Neill, D. Fox, Y. Feng, X. Zhang, B. Jiang, Q. Zhao, H. Zhang, J. N. Coleman, L. Zhang and W. J. Blau, *ACS Nano*, 2013, **7**, 9260–9267.

32 K. F. Mak, C. Lee, J. Hone, J. Shan and T. F. Heinz, *Phys. Rev. Lett.*, 2010, **105**, 136805.

33 L. Yuwen, H. Yu, X. Yang, J. Zhou, Q. Zhang, Y. Zhang, Z. Luo, S. Su and L. Wang, *Chem. Commun.*, 2016, **52**, 529–532.

34 C. Lee, H. Yan, L. E. Brus, T. F. Heinz, J. Hone and S. Ryu, *ACS Nano*, 2010, **4**, 2695–2700.

35 H. Li, Q. Zhang, C. C. R. Yap, B. K. Tay, T. H. T. Edwin, A. Olivier and D. Baillargeat, *Adv. Funct. Mater.*, 2012, **22**, 1385–1390.

36 M. V. Bollinger, K. W. Jacobsen and J. K. Nørskov, *Phys. Rev. B: Condens. Matter Mater. Phys.*, 2003, **67**, 085410.

37 I. Dellien, K. G. McCurdy and L. G. Hepler, *J. Chem. Thermodyn.*, 1976, **8**, 203–207.

38 J. Bi, L. Wu, Y. Zhang, Z. Li, J. Li and X. Fu, *Appl. Catal., B*, 2009, **91**, 135–143.

39 R. Vilaplana, O. Gomis, F. J. Manjon, P. Rodriguez-Hernandez, A. Munoz, D. Errandonea, S. N. Achary and A. K. Tyagi, *J. Appl. Phys.*, 2012, **112**, 103510.

40 W. Du, L. Liu, K. Zhou, X. Ma, Y. Hao and X. Qian, *Appl. Surf. Sci.*, 2015, **328**, 428–435.

41 D. R. Lide, *CRC Handbook of Chemistry and Physics*, CRC Press LLC, 83rd edn, 2002.

42 Y. Wu, X. Cheng, X. Zhang, Y. Xu, S. Gao, H. Zhao and L. Huo, *J. Colloid Interface Sci.*, 2017, **491**, 80–88.

43 A. A. Kumar, A. Som, P. Longo, C. Sudhakar, R. G. Bhuin, S. S. Gupta, Anshup, M. U. Sankar, A. Chaudhary, R. Kumar and T. Pradeep, *Adv. Mater.*, 2017, **29**, 1604260.

44 T. S. Sreeprasad, S. S. Gupta, S. M. Maliyekkal and T. Pradeep, *J. Hazard. Mater.*, 2013, **246**, 213–220.

45 T. S. Sreeprasad, S. M. Maliyekkal, K. P. Lisha and T. Pradeep, *J. Hazard. Mater.*, 2011, **186**, 921–931.